51st AIAA Aerospace Sciences Meeting including the New Horizons Forum and Aerospace Exposition
07 - 10 January 2013, Grapevine (Dallas/Ft. Worth Region), Texas

AIAA 2013-1138

Comparative Study of Algebraic and Transported FSD Models for LES of Premixed Flames in Flamelet and Thin Reaction Zones Regimes

Nasim Shahbazian *, Clinton P.T. Groth † and Ömer L. Gülder ‡

University of Toronto Institute for Aerospace Studies

4925 Dufferin Street, Toronto, ON, M3H 5T6, Canada

A comparative study is performed of two variants of flame surface density (FSD) subfilter-scale (SFS) model, a flamelet-based model for large-eddy simulation (LES) of turbulent premixed combustion. Both algebraic- and transport-equation variants of the FSD flamelet approach were studied so as to investigate the importance of non-equilibrium transport of the flame surface by the turbulence. Six different cases are considered with various turbulence intensities in both lean and stoichiometric turbulent premixed Bunsen flames corresponding to conditions ranging from the upper limit of the flamelet regime to well within the thin reaction zones regime. The predicted LES solutions are compared to the experimental data from a laboratory-scale axisymmetric Bunsen-type premixed turbulent flame. The results of the comparisons highlight weaknesses and strengths of the SFS modelling approaches.

I. Introduction

Large Eddy Simulation (LES) is emerging as a promising computational tool for turbulent combustion processes.[1] However, a considerable complication for LES of turbulent premixed combustion is that chemical reactions occur in a thin reacting layer at extremely small scales that cannot be resolved on LES grids. Accurate subfilter-scale (SFS) modelling of the unresolved scales is therefore required. In this study, both algebraic- and transport-equation variants of the flame surface density (FSD) SFS model, a flamelet-based model for premixed turbulent combustion, are compared and applied to a turbulent Bunsen flame.[2,3] Note that it is both instructive and important to compare algebraic and transported FSD models, as the former are based on equilibrium considerations and the latter incorporate full non-equilibrium transport of the flame surface by the turbulence. Such comparisons can bring to light the relative importance of non-equilibrium transport in turbulent premixed flames.

Although a few comparative studies of LES combustion models for Bunsen flames have been performed recently,[4,5,6] there have been in general few head-to-head comparative studies of FSD SFS modelling approaches. More such studies are certainly needed to advance LES for premixed combustion and clearly identify weaknesses and strengths of the SFS modelling approaches. In this study, the predicted LES solutions for each combustion model are compared to experimental data for a laboratory-scale Bunsen-type premixed turbulent flame. Six flames in four different turbulence intensities in both lean and stoichiometric methane-air flames which have been studied experimentally by Yuen and Gülder,[7] are considered. The six flames correspond to conditions ranging from the upper limit of the flamelet regime to well within the thin reaction zones regime of the standard regime diagram for premixed flames.[8,1,9] The capabilities of each SFS model to predict observed behaviour are examined and compared.

*Ph.D. Candidate, shahbazian@utias.utoronto.ca
†Professor, Senior Member AIAA, groth@utias.utoronto.ca
‡Professor, Associate Fellow AIAA, ogulder@utias.utoronto.ca

II. Large-Eddy Simulation of Turbulent Premixed Flames

The LES framework developed by Lin[10] and Hernández-Pérez *et al.*[6,11] is used for performing this comparative study. This framework is now briefly summarized, along with the SFS combustion models of interest.

A. Favre-Filtered Governing Equations

LES is based on a separation of scales, which is achieved via a low-pass filtering procedure. Scales larger than the filter size, Δ, are resolved, whereas scales smaller than Δ are modelled. Accordingly, a relevant flow parameter, φ, is filtered or Favre-filtered (mass-weighted filtering) to yield $\overline{\varphi}$ or $\widetilde{\varphi}$, respectively. The Favre-filtered form of the Navier-Stokes equations governing compressible flows of a thermally perfect reactive mixture of gases, neglecting Dufour, Soret and radiation effects, is used herein to describe turbulent premixed combustion processes. The equations are given by

$$\frac{\partial\left(\bar{\rho}\right)}{\partial t}+\frac{\partial\left(\bar{\rho}\tilde{u}_i\right)}{\partial x_i}=0\,, \tag{1}$$

$$\frac{\partial\left(\bar{\rho}\tilde{u}_i\right)}{\partial t}+\frac{\partial}{\partial x_j}\left(\bar{\rho}\tilde{u}_i\tilde{u}_j+\delta_{ij}\bar{p}-\check{\tau}_{ij}\right)=\bar{\rho}g_i+A_1\,, \tag{2}$$

$$\frac{\partial(\bar{\rho}\tilde{E})}{\partial t}+\frac{\partial}{\partial x_i}\left[(\bar{\rho}\tilde{E}+\bar{p})\tilde{u}_i+\check{q}_i\right]-\frac{\partial}{\partial x_j}\left(\check{\tau}_{ij}\tilde{u}_i\right)=\bar{\rho}g_i\tilde{u}_i+B_1+B_2+B_3\,, \tag{3}$$

$$\frac{\partial(\bar{\rho}\tilde{Y}_k)}{\partial t}+\frac{\partial(\bar{\rho}\tilde{Y}_k\tilde{u}_i)}{\partial x_i}+\frac{\partial\check{\mathcal{J}}_{k,i}}{\partial x_i}=\overline{\dot{\omega}}_k+C_1\,, \tag{4}$$

where $\bar{\rho}$ is the filtered mixture density, $\tilde{u}_i$ is the Favre-filtered mixture velocity, $\bar{p}$ is the filtered mixture pressure, $\tilde{Y}_k$ is the Favre-filtered mass fraction of species k, $\tilde{E}$ is the Favre-filtered total mixture energy (including chemical energy) given by $\tilde{E}=\sum_{k=1}^{N}\tilde{Y}_k(\check{h}_k+\Delta h^0_{\mathrm{f},k})-\bar{p}/\bar{\rho}+\widetilde{u_iu_i}/2$; $\check{h}_k$, $\Delta h^0_{\mathrm{f},k}$ and $\overline{\dot{\omega}}_k$ are the sensible enthalpy, heat of formation and the filtered reaction rate of species k, respectively, and g_i is the acceleration due to gravity. The filtered equation of state has the form $\bar{p}=\bar{\rho}R\tilde{T}$. The resolved stress tensor, $\check{\tau}_{ij}$, the resolved total heat flux, $\check{q}_i$, and the resolved species diffusive fluxes, $\check{\mathcal{J}}_{k,i}$, are evaluated in terms of the filtered quantities. In this work, the thermodynamic and molecular transport properties of each mixture component are prescribed using the database compiled by Gordon and McBride.[12]

The terms, A_1, B_1, B_2, B_3, and C_1, arise from the low-pass filtering process and require modelling. These terms are expressed as $A_1=-\frac{\partial[\bar{\rho}(\widetilde{u_i\tilde{u}_j}-\tilde{u}_i\tilde{u}_j)]}{\partial x_j}$, $B_1=-\frac{\partial\left[\bar{\rho}(\widetilde{hu_i}-\check{h}\tilde{u}_i)\right]}{\partial x_i}$, $B_2=-\frac{1}{2}\frac{\partial[\bar{\rho}(u_j\widetilde{u_ju_i}-\tilde{u}_j\tilde{u}_j\tilde{u}_i)]}{\partial x_i}$, $C_1=-\frac{\partial\left[\bar{\rho}(\widetilde{Y_ku_i}-\tilde{Y}_k\tilde{u}_i)\right]}{\partial x_i}$, $B_3=-\frac{\partial\left[\sum_{k=1}^{N}\Delta h^0_{\mathrm{f},k}\bar{\rho}(\widetilde{Y_ku_i}-\tilde{Y}_k\tilde{u}_i)\right]}{\partial x_i}$, and must be modelled for closure of the filtered equation set. The subfilter stresses, $\sigma_{ij}=-\bar{\rho}(\widetilde{u_iu_j}-\tilde{u}_i\tilde{u}_j)$, are modelled using an SFS eddy-viscosity type model with $\sigma_{ij}=2\bar{\rho}\nu_{\mathrm{t}}(\check{S}_{ij}-\delta_{ij}\check{S}_{ll}/3)+\delta_{ij}\sigma_{ll}/3$. The SFS turbulent viscosity, ν_{t}, is prescribed herein by using the Smagorinski model.[13] Standard gradient-based approximations are used in this work for the modelling of the SFS fluxes B_1, B_3, and C_1. The subfilter turbulent diffusion term, B_2, is modelled as suggested by Knight *et al.*[14] with $-\bar{\rho}(u_i\widetilde{u_iu_j}-\tilde{u}_i\tilde{u}_i\tilde{u}_j)/2=\sigma_{ij}\tilde{u}_i$.

B. Flame Surface Density Models

As noted in the introduction, a primary challenge in the development of LES for turbulent reactive flows is the accurate and reliable modelling of the interaction between turbulence and chemistry and the specification of the filtered reaction rates, $\overline{\dot{\omega}}_k$. A common approach to the modelling of turbulence/chemistry interactions for premixed flames is offered by flamelet models. In this approach, the internal structure of the flame and detailed chemical kinetics are for the most part ignored and reactive mixture is assumed to be composed of either unburned reactants or burnt products, separated by thin reacting interfaces called flamelets that preserve their locally laminar structure.[8] The primary effect of the turbulence is to wrinkle and strain the embedded laminar flamelets. It is further argued that the flame wrinkling is the main mechanism controlling the turbulent burning rate and/or velocity with the increase in the turbulent flame speed compared to the laminar flame speed simply due to the increase in the flame surface area created by the wrinkling of the flame.[8]

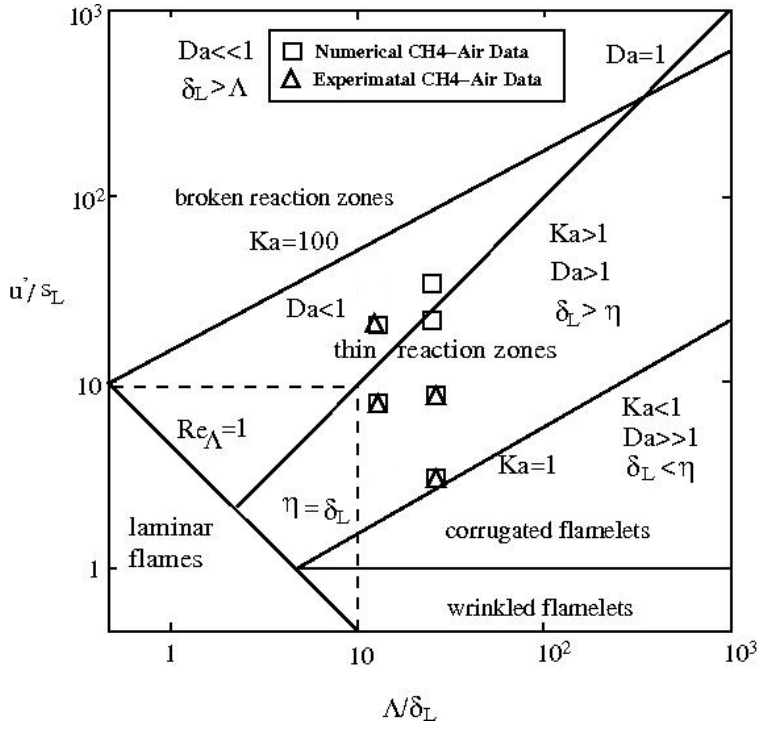

Figure 1: Premixed flame regime diagram showing positions of the premixed flames H, I, J, K, M, and N in the thin reaction zones regime.

Many turbulent premixed combustion models are based on the flamelet concept described above, including FSD-based models. In the FSD approach, the flame front is represented in terms of a reaction progress variable. The progress variable takes on values in the range $0 \leq c \leq 1$ with $c = 0$ in the fresh gases and $c = 1$ in the fully burnt gases and the composition of the reactive mixture is then taken to be fully specified directly in terms of this progress variable. The modelled progress variable equation has the form

$$\frac{\partial\left(\bar{\rho}\tilde{c}\right)}{\partial t} + \frac{\partial\left(\bar{\rho}\tilde{c}\tilde{u}_i\right)}{\partial x_i} = \frac{\partial}{\partial x_i}\left(\frac{\bar{\rho}\nu_\mathrm{t}}{Sc_\mathrm{t}}\frac{\partial\tilde{c}}{\partial x_i}\right) + \rho_\mathrm{r} s_\mathrm{L}\bar{\rho}\tilde{\Sigma}\,, \tag{5}$$

where ρ_r is the density of reactants, s_L is the laminar flame speed, $\tilde{\Sigma}$ is the Favre-filtered flame surface area per unit mass of the mixture, and the product, $\bar{\rho}\tilde{\Sigma}$, is the flame surface area per unit volume or flame surface density. Note that an increase in $\tilde{\Sigma}$ produced by turbulent flame wrinkling results in an increase in the consumption of the progress variable and hence burning rate, in accordance with the flamelet assumption.

The filtered quantity, $\tilde{\Sigma}$, includes contributions from the resolved FSD and the unresolved subfilter-scales. The latter must be modelled. Algebraic models have been considered for the FSD.[2,15,16] Boger *et*

Flame	ϕ	Λ	λ	η	u'	s_L	δ_L	u'/s_L	Λ/s_L	U
CH4-Air		mm	mm	mm	m/s	m/s	mm			m/s
H	1.0	1.635	0.442	0.05174	1.33	0.403	0.05	3.3	32.7	17.59
I	1.0	1.790	0.460	0.02935	2.92	0.403	0.05	7.25	35.8	15.58
J	1.0	1.790	0.460	0.02935	5.79	0.403	0.05	14.38	35.8	15.58
K	1.0	1.790	0.460	0.02935	9.71	0.403	0.05	24.1	35.8	15.58
M	0.7	1.635	0.442	0.05174	1.33	0.201	0.11	6.6	14.86	17.59
N	0.7	1.790	0.460	0.02935	2.92	0.201	0.11	14.38	16.27	15.58

Table 1: Summary of turbulence scales and flame conditions for the six Bunsen-type premixed flames considered herein.

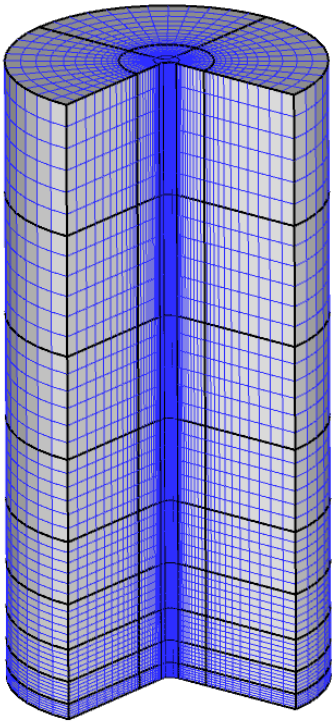

Figure 2: Cylindrical computational domain and mesh containing 1,638,400 cells used in the LES predictions of the turbulent premixed Bunsen flames.

al.[2] suggested the following expression for the SFS flame surface density

$$\tilde{\Sigma} = 4a\frac{\tilde{c}(1-\tilde{c})}{\Delta}\,, \tag{6}$$

where a is a model parameter. While other choices for an algebraic model are certainly possible, this model is considered in the present work and a is assumed to have a constant value of $\sqrt{6/\pi}$.

Models for the FSD based on modelled transport equations are also possible. A modelled transport equation for the FSD was proposed and developed by Hawkes and Cant.[3] This model has been studied quite extensively by Lin[10] and will also be considered herein. The modelled FSD transport equation includes terms representing the production/destruction sources associated with SFS strain and curvature, resolved strain, resolved propagation and curvature and is given by

$$\frac{\partial(\bar{\rho}\tilde{\Sigma})}{\partial t} + \frac{\partial(\bar{\rho}\tilde{u}_i\tilde{\Sigma})}{\partial x_i} - \frac{\partial}{\partial x_i}\left(\frac{\bar{\rho}\nu_{\rm t}}{Sc_{\rm t}}\frac{\partial\tilde{\Sigma}}{\partial x_i}\right) = \Gamma_{\rm K}\bar{\rho}\tilde{\Sigma}\frac{\sqrt{\tilde{k}_\Delta}}{\Delta} - \beta s_{\rm L}\frac{(\bar{\rho}\tilde{\Sigma})^2}{1-\tilde{c}} + (\delta_{ij}-n_{ij})\bar{\rho}\tilde{\Sigma}\frac{\partial\tilde{u}_i}{\partial x_j}$$
$$-\frac{\partial}{\partial x_i}[s_{\rm L}(1+\tau\tilde{c})M_i\bar{\rho}\tilde{\Sigma}] + s_{\rm L}(1+\tau\tilde{c})\bar{\rho}\tilde{\Sigma}\frac{\partial M_i}{\partial x_i}\,, \tag{7}$$

where $\vec{M} = -\nabla\bar{c}/\bar{\rho}\tilde{\Sigma}$ is the flamelet model for the surface averaged normal ($\bar{c}$ is estimated using $\bar{c} = (1+\tau)\tilde{c}/(1+\tau\tilde{c})$), $\alpha = 1 - \vec{M}\cdot\vec{M}$, and $n_{ij} = M_iM_j + 1/3\alpha\delta_{ij}$. The variable $\tau = (T_{\rm ad} - T_{\rm r})/T_{\rm r}$ is the heat release parameter, where $T_{\rm ad}$ and $T_{\rm r}$ are the adiabatic and the reactants temperature, respectively, β is a model constant and must satisfy $\beta \geq 1$ for realisability requirements, α is a resolution factor, and $\Gamma_{\rm K}$ is an efficiency function.[17] The terms on the right hand side of the modelled FSD equation represent the production/destruction sources associated with SFS strain and curvature, resolved strain, resolved propagation and curvature.

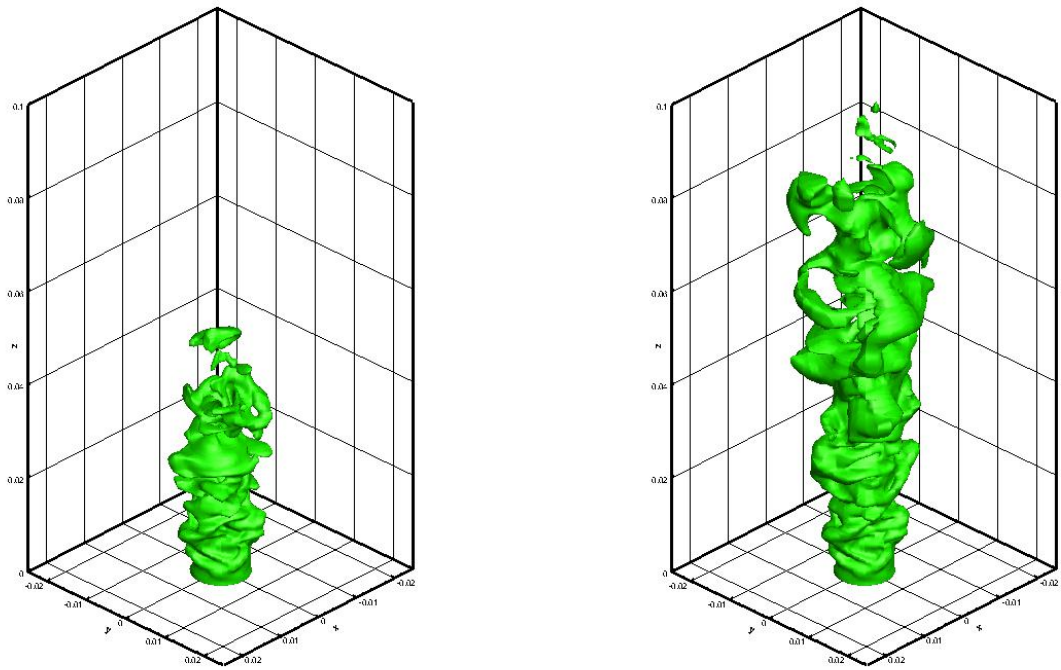

(a) Algebraic FSD, case I

(b) Transported FSD, case I

Figure 3: Instantaneous iso-surfaces of the filtered progress variable, $\tilde{c}=0.5$, at $t=9$ ms after the initiation of the simulations for the stoichiometric premixed Bunsen flame with $u'/s_L = 7.25$ (case I) for algebraic FSD model of Boger *et al.* and transported FSD model of Hawkes and Cant.

C. Finite-Volume Solution Method

The Favre-filtered transport equations described above are solved on multi-block hexahedral meshes employing a second-order accurate parallel finite-volume scheme.[18,19,4,10,6,11] The inviscid flux at each cell face is evaluated using limited linear reconstruction[20] and Riemann-solver based flux functions,[21,22] while the viscous flux is evaluated utilizing a hybrid average gradient-diamond path method.[23] A standard, explicit, two-stage, second-order-accurate, Runge-Kutta, time-marching scheme is used to integrate forward in time the non-linear, coupled-system, of ordinary differential equations resulting from the finite-volume spatial discretization procedure. Parallel implementation of the solution method has been carried out via domain decomposition using the C++ programming language and the MPI (message passing interface) library.[24,25]

III. LES for Bunsen Flames

A. Burner Setup

In what follows, LES solutions obtained with the two different FSD SFS combustion models are contrasted and compared to the experimental data of Yuen and Gülder.[7] Yuen and Gülder considered an axisymmetric Bunsen-type burner with an inner nozzle diameter of 11.2 mm to generate premixed turbulent conical flames stabilized by annular pilot flames. Flame front images were captured using planar Rayleigh scattering achieving a resolution of 45 μm/pixel. The Rayleigh scattering images were converted into temperature field and further processed to provide the temperature gradient and two-dimensional curvature. Particle image velocimetry was used to measure the instantaneous velocity field for the experimental conditions.

In the present study, four of the experimental cases of Yuen and Gülder[7] are considered: two stoichiometric methane-air premixed flames, with an equivalence ratio, ϕ, of $\phi=1$ and relative turbulence intensities of $u'/s_L = 3.3$ (case H) and $u'/s_L = 7.25$ (case I) and two lean methane-air premixed flames with $\phi=0.7$ and relative turbulence intensities of $u'/s_L = 6.55$ (case M) and $u'/s_L = 14.38$ (case N), where u' is the root mean square (RMS) of the turbulent velocity fluctuations. In order to further explore the influence of turbulence on turbulent premixed flame, two additional stoichiometric turbulent premixed flames ($\phi=1$) are

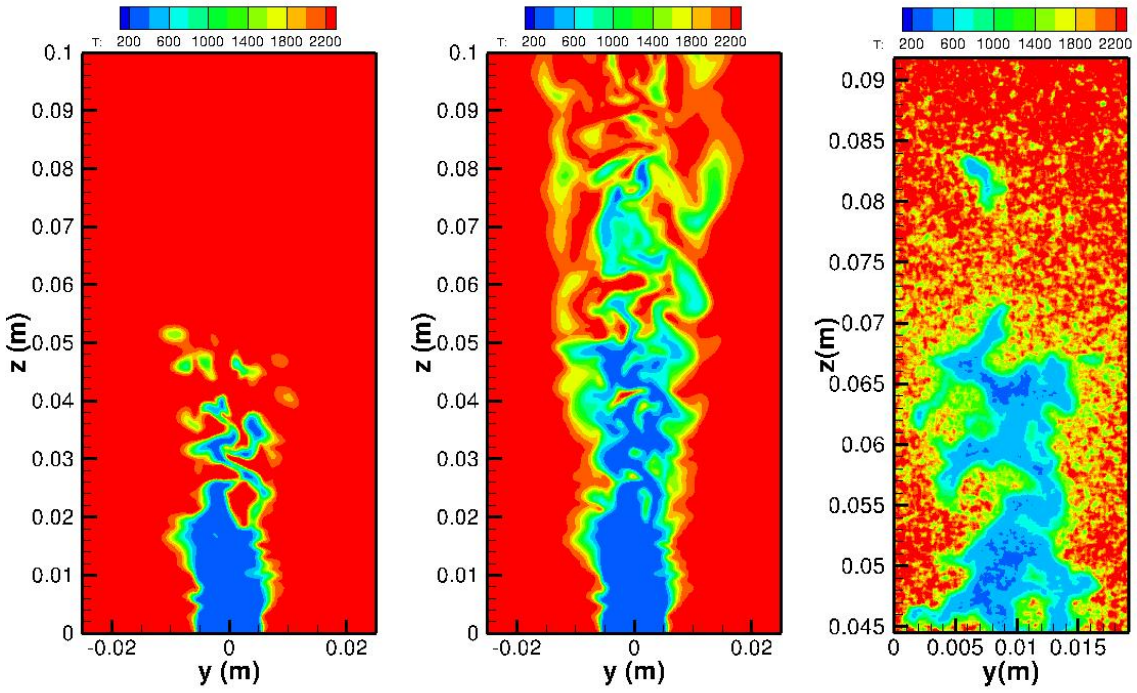

(a) Algebraic FSD (b) Transported FSD (c) Experiment

Figure 4: Predicted contours of the temperature at y-z plane for stoichiometric case with $u'/s_L = 7.25$ (case I) at $t = 9$ ms after the initiation of the simulations of the premixed Bunsen flame for algebraic FSD model of Boger *et al.* (a), transported FSD model of Hawkes and Cant (b), and instantaneous filtered temperature from experimental data (c).

also simulated which are not considered in the experimental work: Case J with relative turbulence intensity of $u'/s_L = 14.38$ and Case K with relative turbulence intensity of $u'/s_L = 24.1$. All these turbulent flames lie either near the upper limit of the flamelet regime or well within the thin-reaction zones region of the standard premixed flame regime diagram.[8,1,9] The turbulence scales and flow conditions for all six of these cases are summarized in Table 1 where Λ, λ, η, and δ_L are the integral length scale, Taylor micro scale, Kolmogorov scale, and laminar flame thickness, respectively, and U is the mean velocity of the reactants at the burner exit plane.

Following the modified approach proposed by Peters,[8] the premixed flame regimes can be of the length scale ratio, Λ/δ_L, and velocity scale ratio, u'/s_L, as shown in Fig. 1. Five different combustion regimes may be identified in the graph. There are the: (i) laminar regime (most practical combustion systems operate in the turbulent regime); (ii) wrinkled flamelet regime in which $u' < s_L$ and the smallest spatial scales of the turbulence, the Kolmogorov scales, η, are larger than the flame front thickness, δ_L, such that the flame front is embedded in the smallest eddies with its laminar structure intact and unaffected by the turbulence; (iii) corrugated flamelet regime in which $u' > s_L$ such that, while the laminar flame structure remains unaffected by the turbulence, the larger turbulent motions are able to induce flame front interactions leading to the formation of pockets of fresh and burnt gases and changes in flame topology; (iv) thin reaction zones regime in which the the Kolmogorov scales are smaller than the flame thickness but larger than the reaction zone and are able to modify the inner laminar flame structure; and (v) broken reaction zones regime in which the turbulent motions have shorter characteristic times than the chemical reaction time and the premixed laminar flame structure is completely disrupted. The position of the six premixed flames of interest herein are also shown on the regime diagram of Fig. 1. The premixed flames H, I, J, K, M, and N all fall within the thin reaction zones regime. Note that flamelet-based combustion models are expected to be valid within both the wrinkled and corrugated flamelet regimes; however, the validity of the flamelet assumption beyond the wrinkled and corrugated flamelet zones and into the thin reaction zones regime remains an open question.

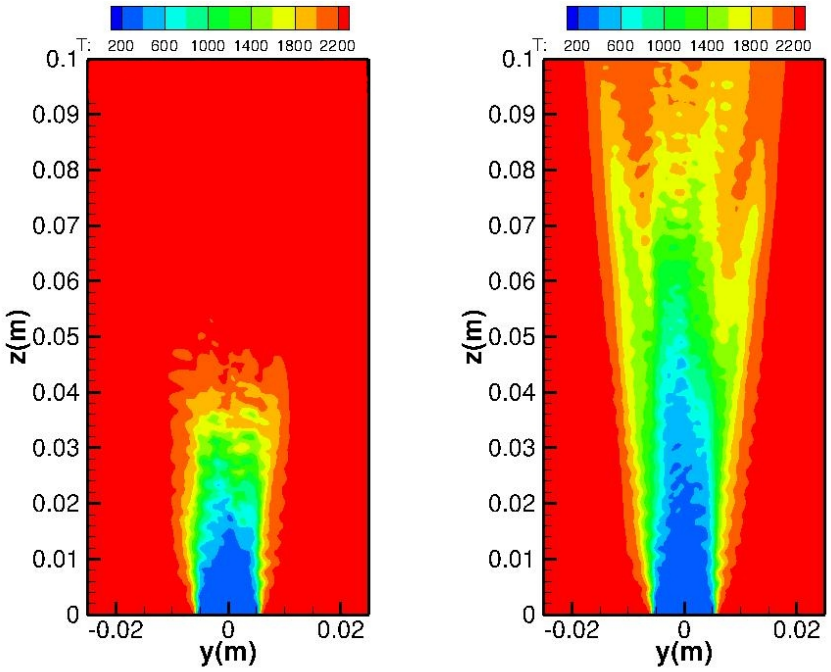

(a) Algebraic FSD (b) Transported FSD

Figure 5: Predicted time-averaged temperature field, $\bar{T}$, stoichiometric case with $u'/s_L = 7.25$ (case I) obtained using algebraic (d) and transported FSD (e) models.

B. LES Setup

For the LES, a cylindrical computational domain having a diameter of 0.05 m and a height of 0.1 m or 0.15 m (depending on the case) was employed and discretized with a grid consisting of 1,638,400 or 2,457,600 hexahedral cells, respectively. The smaller of the two meshes is depicted in Fig. 2. The pilot flame was approximated by a uniform inflow of hot combustion products at a velocity of 16.81 m/s. For the burner exit, a uniform mean inflow of reactants with superimposed turbulent fluctuations was prescribed.

C. Instantaneous Flame Fronts

Three-dimensional views of the predicted instantaneous flame surface, identified by the iso-surface of $\tilde{c}=0.5$, for both algebraic and transported FSD models for case I are displayed in Fig. 3 corresponding to time $t=9$ ms after the initiation of the simulation. At this time, a quasi-steady flame structure has been achieved in each case. Isolated pockets of unburned reactants can be identified higher in the flames. In general, the simulated flames exhibit a highly wrinkled surface with the scale of wrinkling becoming larger near the flame tips. The algebraic and transported FSD model solutions are generally in close agreement with each other up to nearly 2.5-3 cm above the burner rim. Further downstream, greater differences are noticeable. In particular, the flame height for the algebraic FSD model is clearly considerably less than the other model, indicative of a much higher overall predicted turbulent burning rate. While not shown, the same general trends as outlined above for the overall flame structure follow for the other five premixed flames considered in this study, for both stoichiometric and lean cases.

Predicted contours of the temperature in the y-z plane for case I at $t = 9$ ms after the initiation of the simulations for both the algebraic FSD model of Boger *et al.* and transported FSD model of Hawkes and Cant are shown in Fig. 4 (a and b) along with an instantaneous filtered measured temperature field from experimental study (c). The latter was obtained with a filter-width equal to that of the computations. Note that only the upper portion of the flame is depicted in the experimental image. From the figure, it would seem that the numerical simulations are able to reproduce, at least qualitatively, key features of the experimental flame front. Again, the predicted flame height for the algebraic model is considerably shorter than that observed in the experiment.

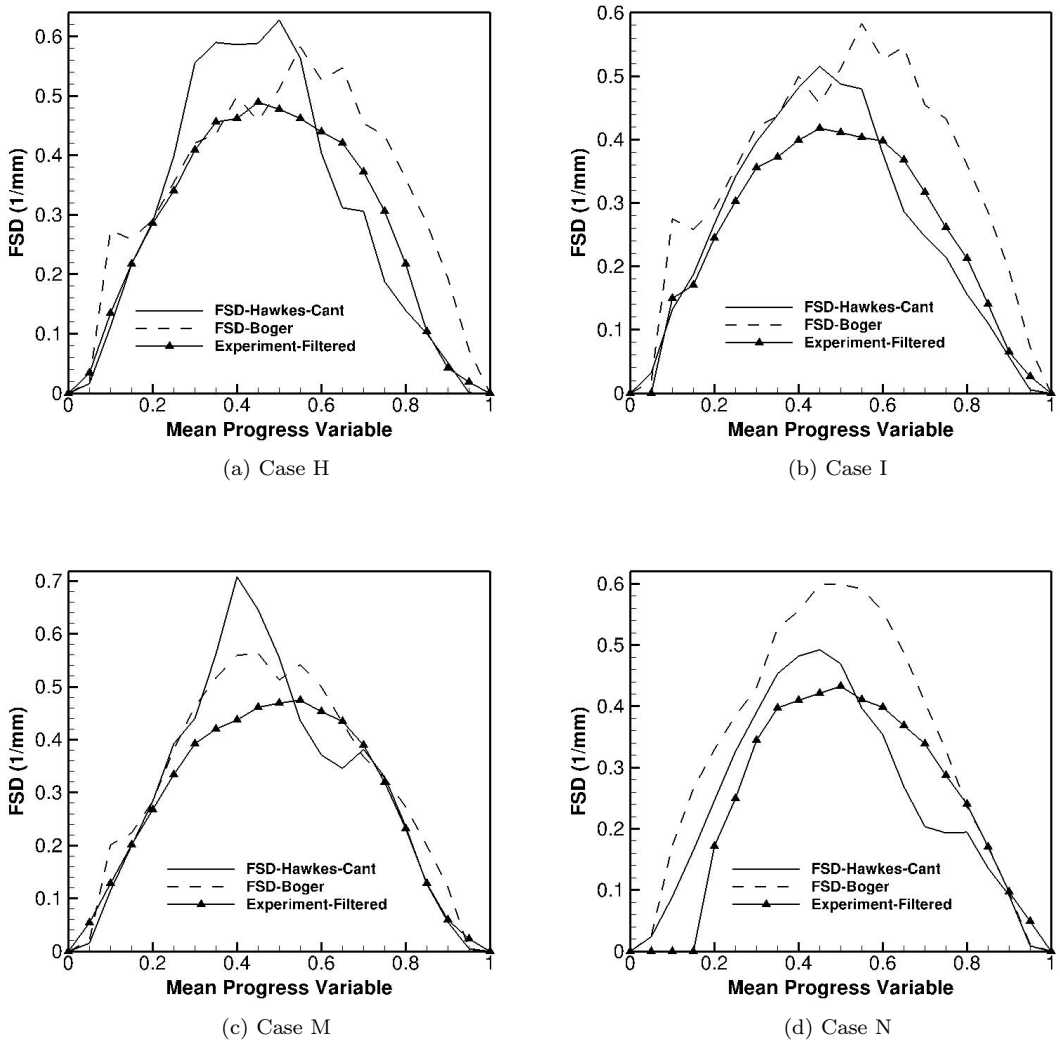

(a) Case H (b) Case I

(c) Case M (d) Case N

Figure 6: Distribution of two-dimensional flame surface density extracted from experimental images and LES results based on instantaneous planar distributions of temperature.

D. Average Flame Structure

Further comparisons of the predicted structure of the Bunsen flame for case I, obtained using each of the two models are depicted in Fig. 5 (a and b), where planar cross sections of the time-averaged temperature field, $\bar{T}$, are shown. The broader flame structure of the transported FSD model flame is fairly evident in the figure and, again, the predicted flame of the algebraic FSD model is considerably shorter than that of the transported FSD model. While results for the other five cases are not shown, the features of the time-averaged flame structure for these flames exhibited, at least qualitatively, quite similar properties.

E. Flame Surface Density

To extract the flame surface density from the experimental data, the Rayleigh scattering images were processed to obtain progress variable fields based on temperature. This progress variable is defined as $c_T = (T - T_\mathrm{u})/(T_\mathrm{b} - T_\mathrm{u})$, where T is the local temperature, T_u is the unburnt gas temperature and T_b is the fully burnt gas temperature. The two-dimensional (2D) maps of the FSD were computed by using the method developed by Shepherd,[26] in which instantaneous flame front edges are superimposed onto the

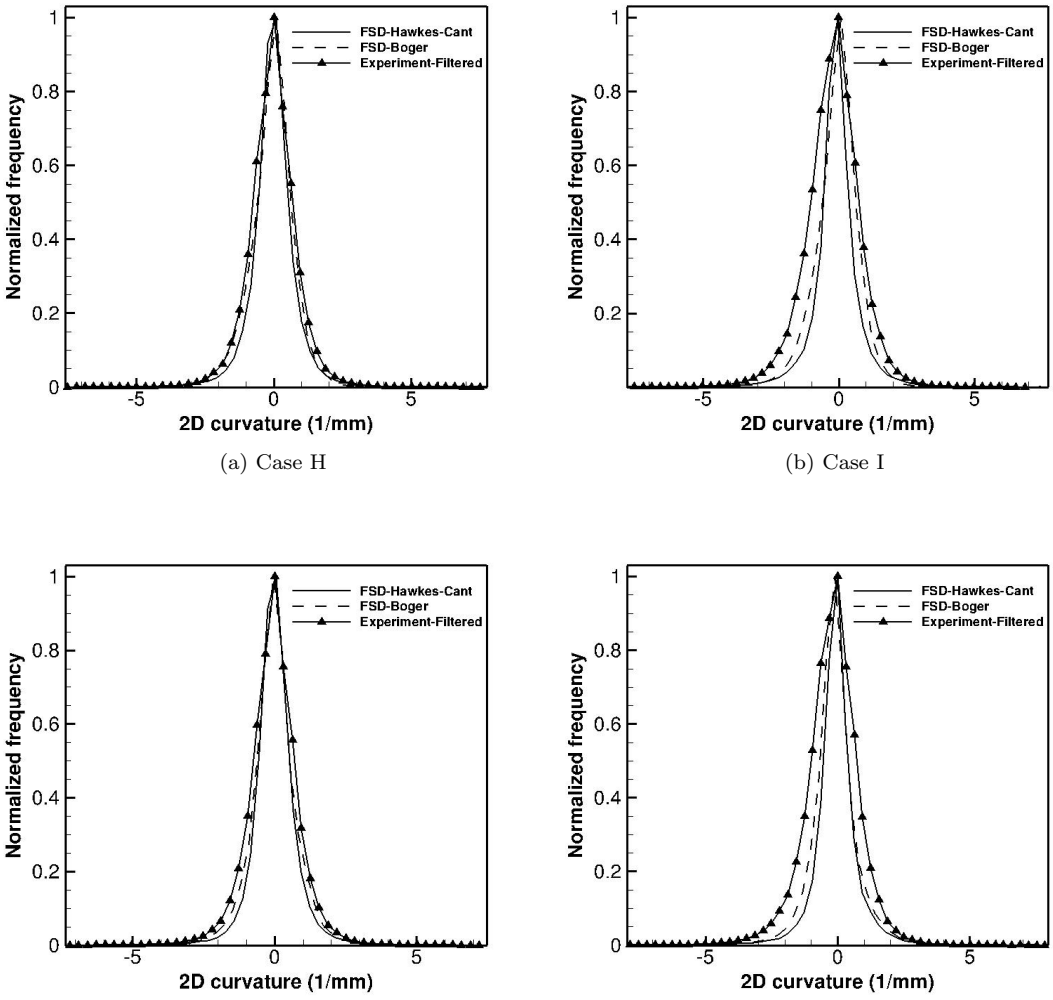

(a) Case H (b) Case I

(c) Case M (d) Case N

Figure 7: Probability Density Functions of two-dimensional flame curvature corresponding to a progress variable $\bar{c}_T = 0.5$.

averaged $\bar{c}_T$ map to calculate the length over area ratio for a given $\bar{c}_T$. The same procedure can and was then applied to 2D slices of the resolved temperature field obtained from the LES simulations. Since LES provides solutions of filtered variables and the resolution of the experimental images is higher than that of the computations, it is more appropriate to compare the numerical results with filtered experimental data. The experimental temperature images were therefore first filtered with a top-hat filter having a characteristic size of two times the average cell size of the LES computational grid as first proposed by Hernández-Pérez *et al.*[6] The total number of post-processed experimental images was 300 and, for each LES simulation, the 2D slices were extracted from 20 instantaneous snapshots of the numerical solution separated by 0.25 ms.

Distributions of the 2D FSD values as a function of the progress variable, $\bar{c}_T$, as extracted from the simulations for four of the cases, are compared directly to similarly processed experimental results in Fig. 6. It can be seen from the figure that, in general, all of the FSD profiles obtained from the LES simulations agree well with the experimental results and, despite some quantitative discrepancies, at least qualitatively reproduce the observed trends. The results for the algebraic and transported FSD models are surprisingly similar and it is difficult to discern significant differences in the predictions. In all of the profiles, the maximum value for the FSD value is around $\bar{c}_T = 0.5$. Moreover, the peak FSD values obtained from the

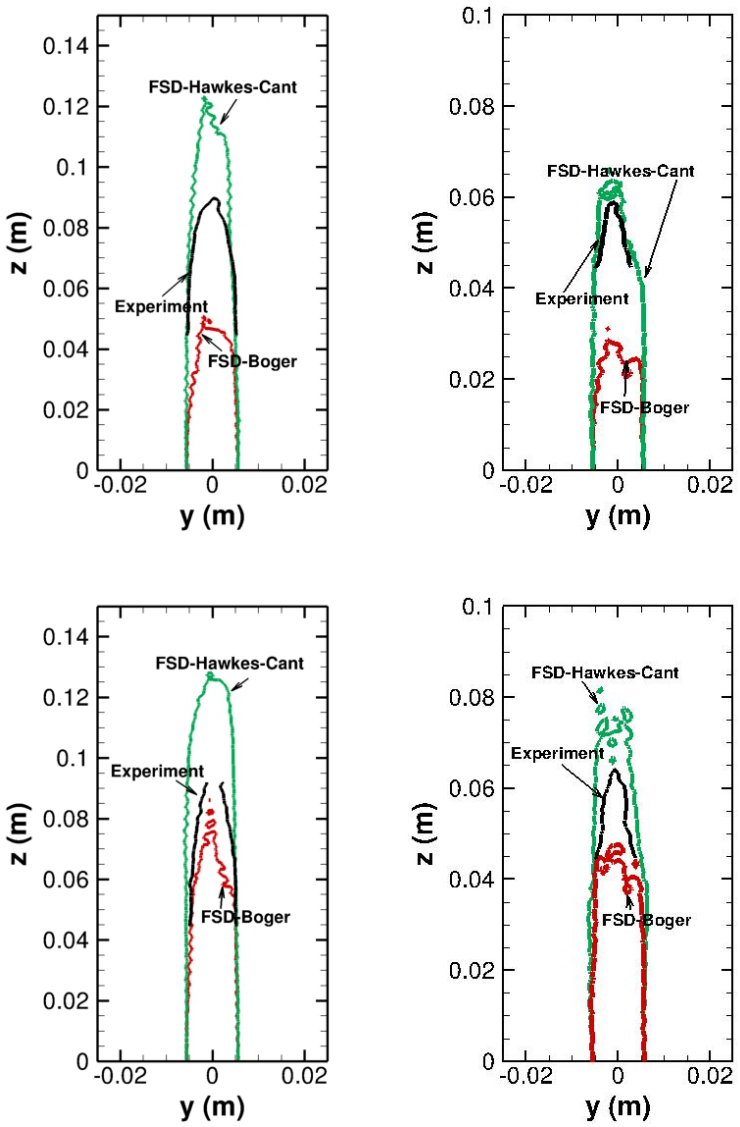

(c) Case M (d) Case N

Figure 8: Estimated averaged flame envelope for algebraic and transported FSD models based on $\bar{c}_T = 0.5$ contour of time-averaged progress variable map.

simulations are slightly higher than the experimental ones.

The two-dimensional flame curvature was also extracted from instantaneous experimental images and slices of the predicted LES temperature. PDFs of flame curvature based on the filtered experimental images and the two FSD models, corresponding to $\bar{c}_T = 0.5$, are shown in Fig. 7. It is quite evident from the figure that all PDFs display a Gaussian-type shape centred around zero with the LES distributions being slightly narrower than the experimental results. Overall, the distributions of curvature for both FSD models are remarkably similar and agree well with filtered experimental results.

F. Flame Heights

Predictions of the average map of $\bar{c}_T = 0.5$, corresponding to the average flame envelope, for algebraic and transported FSD models for flames H, I, M, and N are compared with the map obtained from the Rayleigh scattering images in Fig. 8. It is apparent from the figures that overall, the two FSD combustion models yield flame heights that agree reasonably well with the experimental values in most cases. The experimental

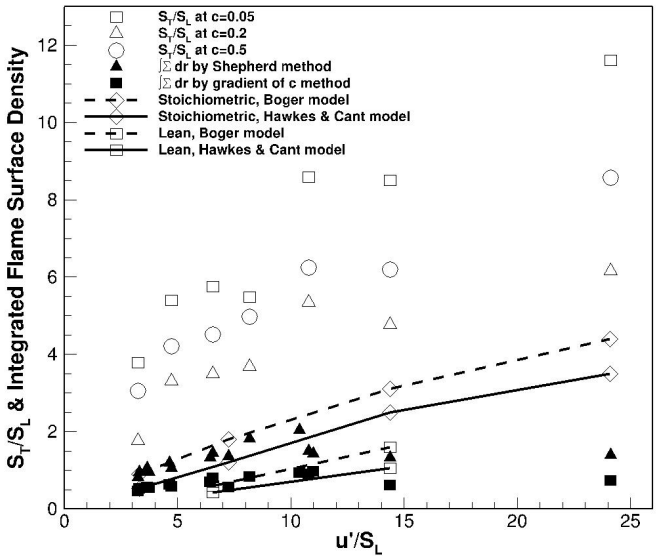

Figure 9: Comparison of predicted and measured values of the normalized turbulent burning rates as a function of turbulence intensity for lean and stoichiometric premixed Bunsen flames.

flame heights for the stoichiometric flames (cases H and I) are 8.5 cm and 6.0 cm, respectively, and the LES modelling with transported FSD predicts flame heights of about 10 cm and 6 cm for these two cases. For the lean cases (cases M and N), the transported FSD model somewhat over predicts the flame heights as compared to the experimental values. The LES results for the algebraic FSD are somewhat inferior to the transported model. In particular, the algebraic model quantitatively under-predicts the average flame height by a considerable margin for the stoichiometric flames, while providing improved predictions for the lean cases. In general, the algebraic model would seem to under-predict the flame height and in comparison to the transported FSD model, it was found that the algebraic model yields much shorter flames for lower turbulence intensities, but as the turbulence intensity increases, the two models show more similar predictions for flame height.

G. Turbulent Burning Rates

The differences in predicted flame heights of the two FSD models is directly related to the overall or total predicted turbulent burning rates. The overall or total predicted turbulent burning rate may be calculated in terms of the integrated FSD as follows

$$\frac{s_{\mathrm{T}}}{s_{\mathrm{L}}} \propto \int_V \bar{\rho}\tilde{\Sigma}\mathrm{d}V \tag{8}$$

where the integration is performed over the entire computational domain. Figure 9 shows a comparison of the predicted quasi-steady normalized turbulent burning rates for the six premixed flames to estimated values of the burning rates and integrated flame surface area obtained by Yuen and Gülder[7] from analysis of the mean flame brush.

It is evident from the figure that the LES predictions of burning rate for both FSD models show a gradual increase as a function of turbulence intensity, but this increase is somewhat below the experimentally measured values, as is the overall burning rate. The burning rates predicted by the two FSD models are qualitatively quite similar, but the overall burning rate of the algebraic model is about 1.4 times higher than that of the transported FSD model. As the two FSD models invoke the flamelet assumption of Damköhler, the predicted burning rates seem to agree well with the measurements of flame area for lower turbulence intensities.

IV. Concluding Remarks

The present study of subfilter-scale models for LES of turbulent premixed methane-air Bunsen flames has permitted a comparison of algebraic and transported FSD models. The comparison has revealed that, for premixed turbulent flames in the upper flamelet and thin-reaction zones regimes, the algebraic FSD model of Boger *et al.*[2] can greatly over-predict the turbulent burning rate, flame height, and flame area compared with experiment, particularly for the relatively lower turbulence intensity cases. For the higher-turbulence intensities, the algebraic model predictions are somewhat improved and some tuning of model constants may be possible for improved results. In contrast, the transported FSD of Hawkes and Cant[3] provides considerably improved predictions, providing results that agree both qualitatively and quantitatively with key aspects of the observed flame structure and behaviour. Future research will involve further comparisons of the algebraic and transported SFS models for premixed flames over a wider range of turbulence intensities and flame conditions.

Acknowledgments

Financial support for the research described herein was provided by the MITACS (Mathematics of Information Technology and Complex Systems) Network, part of the Networks of Centres of Excellence (NCE) program funded by the Canadian government. This funding is gratefully acknowledged with many thanks. Computational resources for performing all of the calculations reported herein were provided by the SciNet High Performance Computing Consortium at the University of Toronto and Compute/Calcul Canada through funding from the Canada Foundation for Innovation (CFI) and the Province of Ontario, Canada.

References

[1]Pitsch, H., "Large-Eddy Simulation of Turbulent Combustion," *Ann. Rev. Fluid Mech.*, Vol. 38, 2006, pp. 453–482.

[2]Boger, M., Veynante, D., Boughanem, H., and Trouvé, A., "Direct numerical simulation analysis of flame surface density concept for large eddy simulation of turbulent premixed combustion," *Proceedings of Combustion Institute*, Vol. 27, 1998, pp. 917–925.

[3]Hawkes, E. R. and Cant, R. S., "Implications of a Flame Surface Density Approach to Large Eddy Simulation of Premixed Turbulent Combustion," *Combust. Flame*, Vol. 126, 2001, pp. 1617–1629.

[4]Lin, W., Hernández-Pérez, F. E., Groth, C. P. T., and Gülder, O. L., "Comparison of Subfilter Scale Models for LES of Turbulent Premixed Flames," Paper 2008-1048, AIAA, January 2008.

[5]De, A. and Acharya, S., "Large eddy simulation of a premixed bunsen flame using a modified thickened-flame model at two Reynolds number," *Combust. Sci. Tech.*, Vol. 181, 2009, pp. 1231–1272.

[6]Hernández-Pérez, F. E., Yuen, F. T. C., Groth, C. P. T., and Gülder, O. L., "LES of a Laboratory-Scale Turbulent Premixed Bunsen Flame Using FSD, PCM-FPI and Thickened Flame Models," *Proc. Combust. Inst.*, Vol. 33, 2011, pp. 1365–1371.

[7]Yuen, F. T. C. and Gülder, O. L., "Premixed turbulent flame front structure investigation by Rayleigh scattering in the thin reaction zone regime," *Proceedings of Combustion Institute*, Vol. 32, 2009, pp. 1747–1754.

[8]Peters, N., *Turbulent Combustion*, Cambridge University Press, Cambridge, 2000.

[9]Düsing, M., Sadiki, A., and Janicka, J., "Towards a Classification of Models for the Numerical Simulation of Premixed Combustion Based on a Generalized Regime Diagram," *Combust. Theory Modelling*, Vol. 10, No. 1, 2006, pp. 105–132.

[10]Lin, W., *Large-Eddy Simulation of Premixed Turbulent Combustion Using Flame Surface Density Approach*, Ph.D. thesis, University of Toronto, August 2010.

[11]Hernández-Pérez, F. E., *Subfilter Scale Modelling for Large Eddy Simulation of Lean Hydrogen-Enriched Turbulent Premixed Combustion*, Ph.D. thesis, University of Toronto, April 2011.

[12]Gordon, S. and McBride, B. J., "Computer Program for Calculation of Complex Chemical Equilibrium Compositions and Applications I. Analysis," Reference Publication 1311, NASA, 1994.

[13]Smagorinski, J., "General Circulation Experiments with te Primitive Equations. I: The Basic Experiment," *Monthly Weather Review*, Vol. 91, No. 3, 1979, pp. 99–165.

[14]Knight, D., Zhou, G., Okong'o, N., and Shukla, V., "Compressible Large Eddy Simulation Using Unstructured Grids," Paper 98-0535, AIAA, January 1998.

[15]Charlette, F., Meneveau, C., and Veynante, D., "A power-law flame wrinkling model for LES of premixed turbulent combustion, part I: non-dynamic formulation and initial tests," *Combust. Flame*, Vol. 131, 2002, pp. 159–180.

[16]Angelberger, C., Veynante, D., and Poinsot, T., "Large eddy simulations of combustion instabilities in premixed flames," Proceedings of the Summer Program, Center for Turbulence Research, 1998.

[17]Meneveau, C. and Poinsot, T., "Stretching and quenching of flamelets in premixed turbulent combustion," *Combust. Flame*, Vol. 86, 1991, pp. 311–332.

[18]Gao, X. and Groth, C. P. T., "Parallel Adaptive Mesh Refinement Scheme for Three-Dimensional Turbulent Non-Premixed Combustion," Paper 2008-1017, AIAA, January 2008.

[19]Gao, X. and Groth, C. P. T., "A Parallel Solution-Adaptive Method for Three-Dimensional Turbulent Non-Premixed Combusting Flows," *J. Comput. Phys.*, Vol. 229, No. 5, 2010, pp. 3250–3275.

[20]Barth, T. J., "Recent Developments in High Order K-Exact Reconstruction on Unstructured Meshes," Paper 93-0668, AIAA, January 1993.

[21]Roe, P. L., "Approximate Riemann Solvers, Parameter Vectors, and Difference Schemes," *J. Comput. Phys.*, Vol. 43,

1981, pp. 357–372.
[22]Liou, M.-S., "A Sequel to AUSM, Part II: AUSM$^+$-up for all Apeeds," *J. Comput. Phys.*, Vol. 214, 2006, pp. 137–170.
[23]Mathur, S. R. and Murthy, J. Y., "A Pressure-Based Method for Unstructured Meshes," *Numerical Heat Transfer*, Vol. 31, 1997, pp. 191–215.
[24]Gropp, W., Lusk, E., and Skjellum, A., *Using MPI*, MIT Press, Cambridge, Massachussets, 1999.
[25]Gropp, W., Lusk, E., and Thakur, R., *Using MPI-2*, MIT Press, Cambridge, Massachussets, 1999.
[26]Shepherd, I., "Flame Surface Density and Burning Rate in Premixed Turbulent Flames," *Proceedings of Combustion Institute*, Vol. 26, 1996, pp. 373–379.